


Prostate cancer assessment using MR elastography of fresh prostatectomy specimens at 9.4 T

Rolf Reiter^{1,2}  | Shreyan Majumdar¹ | Steven Kearney¹ | Andre Kajdacsy-Balla³ |
Virgilia Macias³ | Simone Crivellaro⁴ | Brandon Caldwell⁴ | Michael Abern⁴ |
Thomas J. Royston¹ | Dieter Klatt¹

¹Richard and Loan Hill Department of Bioengineering, University of Illinois at Chicago, Chicago, Illinois

²Department of Radiology, Charité – Universitätsmedizin Berlin, corporate member of Freie Universität Berlin, Humboldt-Universität zu Berlin, and Berlin Institute of Health, Berlin, Germany

³Department of Pathology, University of Illinois at Chicago, Chicago, Illinois

⁴Department of Urology, University of Illinois at Chicago, Chicago, Illinois

Correspondence

Rolf Reiter, Department of Radiology,
Charité – Universitätsmedizin Berlin,
Charitéplatz 1, 10117 Berlin, Germany.
Email: rolf.reiter@charite.de

Funding information

Deutsche Forschungsgemeinschaft
(DFG, German Research Foundation):
RE 4161/1-1, RE 4161/1-2, RE 4161/2-1
(Rolf Reiter)

Purpose: Despite its success in the assessment of prostate cancer (PCa), in vivo multiparametric MRI has limitations such as interobserver variability and low specificity. Several MRI methods, among them MR elastography, are currently being discussed as candidates for supplementing conventional multiparametric MRI. This study aims to investigate the detection of PCa in fresh ex vivo human prostatectomy specimens using MR elastography.

Methods: Fourteen fresh prostate specimens from men with clinically significant PCa without formalin fixation or prior radiation therapy were examined by MR elastography at 500 Hz immediately after radical prostatectomy in a 9.4T preclinical scanner. Specimens were divided into 12 segments for both calculation of storage modulus (G' in kilopascals) and pathology (Gleason score) as reference standard. Sensitivity, specificity, and area under the receiver operating characteristic curve were calculated to assess PCa detection.

Results: The mean G' and SD were as follows: all segments, 8.74 ± 5.26 kPa; healthy segments, 5.44 ± 4.40 kPa; and cancerous segments, 10.84 ± 4.65 kPa. The difference between healthy and cancerous segments was significant with $P \leq .001$. Diagnostic performance assessed with the Youden index was as follows: sensitivity, 69%; specificity, 79%; area under the curve, 0.81; and cutoff, 10.67 kPa.

Conclusion: Our results suggest that prostate MR elastography has the potential to improve diagnostic performance of multiparametric MRI, especially regarding its 2 major limitations: interobserver variability and low specificity. Particularly the high value for specificity in PCa detection is a stimulating result and encourages further investigation of this method.

This is an open access article under the terms of the Creative Commons Attribution-NonCommercial License, which permits use, distribution and reproduction in any medium, provided the original work is properly cited and is not used for commercial purposes.

© 2019 The Authors. *Magnetic Resonance in Medicine* published by Wiley Periodicals, Inc. on behalf of International Society for *Magnetic Resonance in Medicine*

KEYWORDS

MR elastography, prostate cancer, prostatectomy specimens

1 | INTRODUCTION

Despite its success in the assessment of prostate cancer (PCa), *in vivo* multiparametric MRI (mpMRI) suffers from limitations such as interobserver variability and low specificity.^{1,2} Specifically, the differentiation of benign prostatic hyperplasia nodules from malignant tumors and the low sensitivity to detect extraprostatic tumor extension into surrounding neurovascular structures remain major obstacles. Although PCa is the second most common cancer in men worldwide, most men with diagnosed PCa will die of other causes.³ Due to this gap between incidence and mortality, accurate risk stratification for identification of clinically significant PCa versus indolent PCa is desirable for clinical management, especially to select men for radical prostatectomy or active surveillance. The current clinical reference standard for staging PCa is histopathological analysis of transrectal ultrasound-guided core needle biopsy specimens typically taken from 12 different locations. However, this biopsy scheme is known to frequently underestimate Gleason scores (GS) and miss tumors especially in the anterior gland and apex.^{4,5}

Magnetic resonance elastography (MRE) is a noninvasive method to quantify mechanical tissue properties. Previous studies investigating MRE of *ex vivo* prostates were performed in specimens with formalin fixation or prior radiation therapy, which are both known to substantially alter mechanical tissue properties.⁶⁻¹⁰ In comparison to MRE examinations of other organs such as liver or brain, the small prostate size and shear wave attenuation by surrounding tissue make it more challenging to generate shear waves with sufficient amplitudes while at the same time ensuring patient comfort.⁸ Previous pilot studies investigated various experimental approaches, including transurethral, endorectal, and transperineal mechanical actuator setups in animals and humans.¹¹⁻¹³ To overcome current technical challenges and to explore the potential of prostate MRE, we used an *ex vivo* approach to characterize mechanical properties of human prostatectomy specimens. We aimed to assess the detection of PCa in fresh specimens without formalin fixation or prior radiation therapy using MRE at 9.4 T and whole-mount pathology or biopsy as a reference standard.

2 | METHODS**2.1 | Subjects**

The study was approved by the University of Illinois at Chicago institutional review board, and written informed

consent was obtained from all subjects. Prostate specimens of 14 men were examined in this prospective monocenter study. Inclusion criteria were men with a clinical indication for radical prostatectomy for PCa and age of 40 to 79 years. Exclusion criteria were preoperative hormone therapy, preoperative pelvic surgery, prior radiation therapy, and lack of adequate histopathology data to confidently localize the tumors. All radical prostatectomies were performed by robot assistance with en bloc removal of prostate and seminal vesicles by 1 of 2 experienced urologic surgeons (M.A. and S.C.). After surgery was performed, a small fiducial filled with 2% agarose gel was sewed to the prostate in an anterior and mid-sagittal plane to maintain spatial orientation (Figure 1A). Additionally, an 18-French silicone catheter was placed in the urethral lumen.

2.2 | Magnetic resonance elastography

Immediately after radical prostatectomy, fresh prostate specimens without formalin fixation were examined by

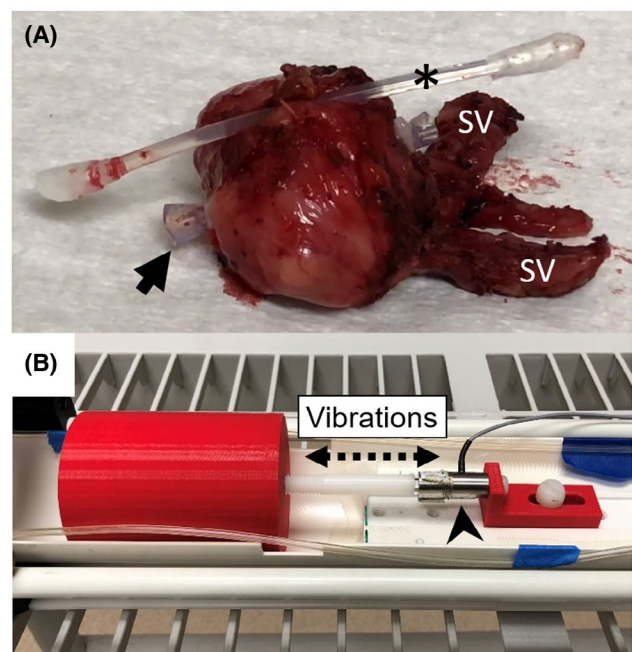


FIGURE 1 A, Excised prostatectomy specimen with seminal vesicles (SV). A fiducial (asterisk) was sewed to the top of the prostate, and a catheter was placed inside the urethra (arrow). B, Magnetic resonance elastography setup with piezoelectric actuator (arrowhead) and cylindrical tube (red), into which the prostate was placed. The dashed arrow indicates the direction of vibrations

MRE in a 9.4T MRI scanner (310/ASR; Agilent, Santa Clara, California) with a 62-mm inner diameter quadrature birdcage RF coil at room temperature (23°C). The prostates were placed inside a cylindrical tube (Figure 1B). To account for different prostate sizes and to maximize wave amplitudes, paper towels were used to ensure full 360° contact of the organ with the tube. A piezoelectric actuator (P-840.1; Physik Instrumente, Karlsruhe, Germany) was attached to the tube and induced radially converging shear waves in the sample using a drive frequency of 500 Hz. One specimen (No. 3) had to be examined at 250 Hz because shear wave attenuation was too high at 500 Hz for this specific sample. To account for differences in prostate volume, geometry, and tissue properties, MRE sequence parameters were adjusted for every specimen individually to optimize resolution while maintaining a 2-hour period from the operating room to pathology. Scan parameters for all specimens are listed in Table 1. Magnetic resonance elastography was performed using a modified spin-echo pulse sequence based on sample interval modulation MRE for the simultaneous acquisition of wave field displacement along all 3 Cartesian directions, as described in Refs ¹⁴ and ¹⁵. The average MRE scan time was 34 minutes.

2.3 | Image processing

Complex wave images of each displacement component at the mechanical frequency used were calculated by applying a discrete Fourier transform along the 12 acquired time steps and extraction of the first harmonic. Images of complex shear modulus G^* , with its real (G') and imaginary (G'') part representing the storage and loss modulus, respectively, were calculated from the noise-filtered complex wave images after application of the curl operator by inverting the overdetermined Helmholtz equation in a least-squares manner.^{15,16} Masks were generated to divide prostates into 12 segments (right/left, base/mid/apex, anterior/posterior) and to calculate segment-based averages of G' and G'' . A 3-pixel erosion was applied to the edge of the outer prostate contour and urethra to avoid boundary effects.

2.4 | Reference standard

All patients underwent clinically indicated preoperative imaging-guided biopsies from all 12 segments as diagnostic reference standard, and the presence of any cancer ($GS \geq 6$) was reported. Additionally, whole-mount pathology was performed in 8 radical prostatectomy specimens as the most accurate reference standard available. Prostate specimens were injected with formalin for fixation after the MRE measurements were performed and within 2 hours after surgery.

TABLE 1 Scan parameters

Prostate	1	2	3	4	5	6	7	8	9	10	11	12
Matrix	128 × 128	96 × 96	64 × 64	128 × 128	128 × 128	64 × 64	64 × 64	64 × 64	64 × 64	64 × 64	64 × 64	64 × 64
FOV (mm × mm)	40 × 40	48 × 48	64 × 64	42 × 42	64 × 64	60 × 60	64 × 64	64 × 64	64 × 64	64 × 64	64 × 64	64 × 64
Resolution (mm)	0.3125	0.5	1	0.3281	0.5	0.9375	1	1	1	1	1	1
Slice thickness (mm)	2	2	1	1	1	2	1	1	1	2	1	1
Number of slices	20	20	50	56	45	30	64	60	30	22	34	38
TR (ms)	750	700	2400	2200	2000	1250	2200	2500	1500	1000	1500	1500
TE (ms)	25.2	26.1	25.5	27.6	27.6	27.3	19.4	27.4	23.4	23.3	23.4	23.4
Number of MEGs	8	10	4	10	10	10	6	10	8	8	8	8
Frequency (Hz)	500	500	250	500	500	500	500	500	500	500	500	500
Scan time (minutes)	25	18	41	76	68	21	28	42	25	17	25	25

Abbreviations: MEG, motion-encoding gradient.

Paraffin-embedded slices were obtained perpendicular to the urethral axis from apex to base every 3–4 mm. Slides were stained with hematoxylin and eosin and digitized by a whole-slide scanner (Aperio Scanscope AT2; Leica Biosystems, Nussloch, Germany) at $\times 20$ magnification and 0.5 $\mu\text{m}/\text{pixel}$ resolution. Tumor regions were annotated on the digitized hematoxylin and eosin–stained and CD31–stained slides (Aperio ImageScope). Gleason scores were determined for each slice and segment to categorize cancer as low-grade ($\text{GS} = 6$), intermediate-grade ($\text{GS} = 7$), or high-grade ($\text{GS} = 8$ and 9) PCa according to the 2014 recommendations of the International Society of Urological Pathology.¹⁷ Segment-based averages of G' and G'' were compared with biopsy findings and whole-mount pathology to determine the diagnostic performance.

2.5 | Statistical data analysis

The Shapiro-Wilk test was used to assess the normal distribution of G' and G'' for all segments. The Wilcoxon rank sum test was used to assess differences between healthy and cancerous segments. Pearson's correlation coefficient (R) was calculated for pairwise comparison of the most important parameters (G' , G'' , GS , age, prostate volume, proportion of tissue involved by tumor). The level of significance for all tests was $P \leq .05$. Optimized values for sensitivity, specificity, negative and positive predictive values, and area under the receiver operating characteristic curve (AUC) with 95% confidence intervals were calculated using the Youden index to assess the diagnostic performance of G' for PCa detection. Statistical analysis was performed using *MATLAB* version 9.0 R2016a (The MathWorks, Natick, Massachusetts).

3 | RESULTS

A total of 14 men with clinically significant PCa were included in this study. MRE failed in 2 prostates due to technical difficulties with the custom-designed piezoelectric actuator. Analyses were conducted for the entire cohort (12 patients with 144 individual prostate segments) and for a subgroup with whole-mount pathology (8 patients with 96 individual prostate segments). The prostate specimens were from men with a mean age of 62 years and a range from 47 to 75 years. Further patient characteristics are compiled in Table 2.

3.1 | Magnetic resonance elastography

Figure 2 shows an exemplary case with preoperative in vivo mpMRI, ex vivo MRE, and whole-mount pathology. Unlike mpMRI, ex vivo MRE magnitude images do not allow clear differentiation of anatomic zones in the prostate. Data were not distributed normally ($P \leq .001$). Therefore, in addition to the mean values, median values of G' and G'' for the entire cohort and subgroup with whole-mount pathology are listed in Table 3. Additionally, box-plots are shown in Figure 3.

For the entire cohort, the mean G' and SD were as follows: all segments ($N = 144$), 8.74 ± 5.26 kPa; healthy segments ($N = 56$), 5.44 ± 4.40 kPa; and cancerous segments ($N = 88$), 10.84 ± 4.65 kPa. A statistically significant difference between healthy and cancerous segments was evident for both G' and G'' with $P \leq .001$. Mean prostate volume was 27 mL, ranging from 16 to 63 mL. No significant correlation was found between G' and the following parameters: age ($R = -0.02$; $P = .95$), prostate volume

TABLE 2 Patient characteristics

Patient	Age (years)	Prostate volume (mL)	Tumor proportion (%)	Reference method	Gleason score	Clinical stage
1	60	24	30	Biopsy	4 + 3	pT3a
2	69	29	15	Biopsy	3 + 4	pT2c
3	60	63	1	Biopsy	3 + 4	pT2a
4	59	16	5	Biopsy	3 + 4	pT2c
5	58	31	10	Whole-mount pathology	4 + 5	pT2c
6	52	28	13	Whole-mount pathology	3 + 3	pT2c
7	66	25	70	Whole-mount pathology	4 + 3	pT3a
8	47	24	10	Whole-mount pathology	5 + 4	pT3a
9	64	21	10	Whole-mount pathology	3 + 4	pT3a
10	72	21	7	Whole-mount pathology	3 + 4	pT3a
11	58	25	10	Whole-mount pathology	4 + 5	pT3b
12	75	21	17	Whole-mount pathology	3 + 4	pT3a

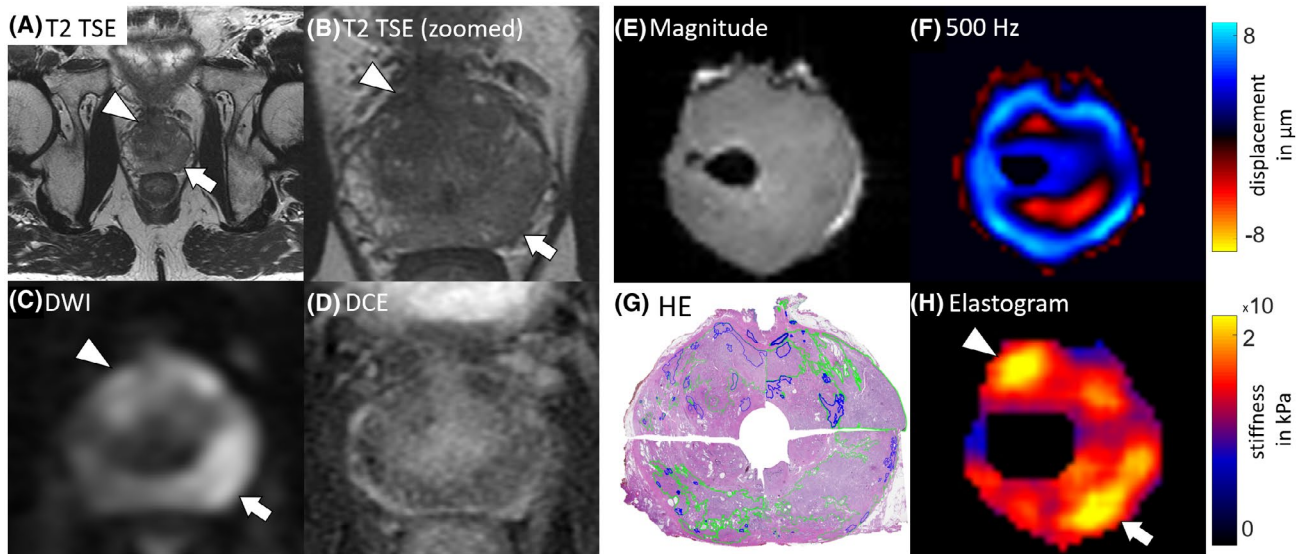


FIGURE 2 Axial plane through the midgland of a patient with prostate cancer. In vivo: A,B, T₂ turbo spin echo (TSE) image with an extensive hypointensity in the left peripheral zone (arrow) and in the right and left transition zone (arrowhead). C, Diffusion-weighted imaging with $b = 2000 \text{ s/mm}^2$. The markedly hyperintense signal corresponds to the low T₂ signal in (A) and (B). D, No abnormal signal increase is seen in the DCE sequence. Ex vivo: E, Magnitude image. F, Phase image scaled to shear wave displacement. G, The marked-up hematoxylin and eosin (HE) image depicts a tumor with a Gleason score of 3 + 4 = 7 (green, Gleason pattern 3; blue, Gleason pattern 4). H, Map of storage modulus (bright colors indicate the tumor with an increased shear stiffness)

TABLE 3 Overview mean and median values

Segments	G' in kPa			G'' in kPa		
	Mean	Median	SD	Mean	Median	SD
Entire cohort (12 patients)						
All ($N = 144$)	8.74	10.95	5.26	4.46	4.57	2.64
Healthy ($N = 56$)	5.44	3.08	4.40	2.92	1.95	2.16
Any cancer ($N = 88$)	10.84	12.58	4.65	5.45	6.03	2.43
Subgroup with whole-mount pathology (8 patients)						
All ($N = 96$)	11.83	12.58	3.53	5.92	6.21	2.00
Healthy ($N = 22$)	10.08	11.54	3.60	5.13	5.76	1.88
Any cancer ($N = 74$)	12.36	12.91	3.34	6.15	6.50	1.98
GS 6 ($N = 16$)	11.73	12.71	3.30	5.80	6.61	1.78
GS 7 ($N = 36$)	12.64	13.32	3.25	6.30	6.67	1.94
GS 8/9 ($N = 22$)	12.34	12.84	3.46	6.16	6.21	2.13

Note: G' and G'' are the real and imaginary part of the complex shear modulus, respectively.

($R = -0.34$; $P = .29$), and proportion of tissue involved by tumor ($R = 0.25$; $P = .43$).

For the subgroup with whole-mount pathology, the mean G' and SD were as follows: all segments ($N = 96$), $11.83 \pm 3.53 \text{ kPa}$; healthy segments ($N = 22$), $10.08 \pm 3.60 \text{ kPa}$; and cancerous segments ($N = 74$), $12.36 \pm 3.34 \text{ kPa}$. A significant difference between healthy and cancerous segments was evident for G' ($P \leq .003$) but not for G'' ($P = .06$). Moreover, there were no significant differences between low-grade, intermediate-grade, and high-grade PCa (Figure 3C). The AUC

values decreased with increasing GS (Table 4). A weak correlation between G' and GS ($R = 0.24$, $P = .02$), but no correlation between G'' and GS ($R = 0.13$, $P = .21$) was found.

Optimized values of diagnostic performance of G' using the Youden index are compiled in Table 4. Overall, the best diagnostic performance was found for the entire cohort for the detection of any PCa (GS ≥ 6) with an AUC of 0.81 (sensitivity, 69%; specificity, 79%; cutoff, 10.67 kPa). The corresponding receiver operating characteristic curve with 95% confidence intervals is shown in Figure 4.

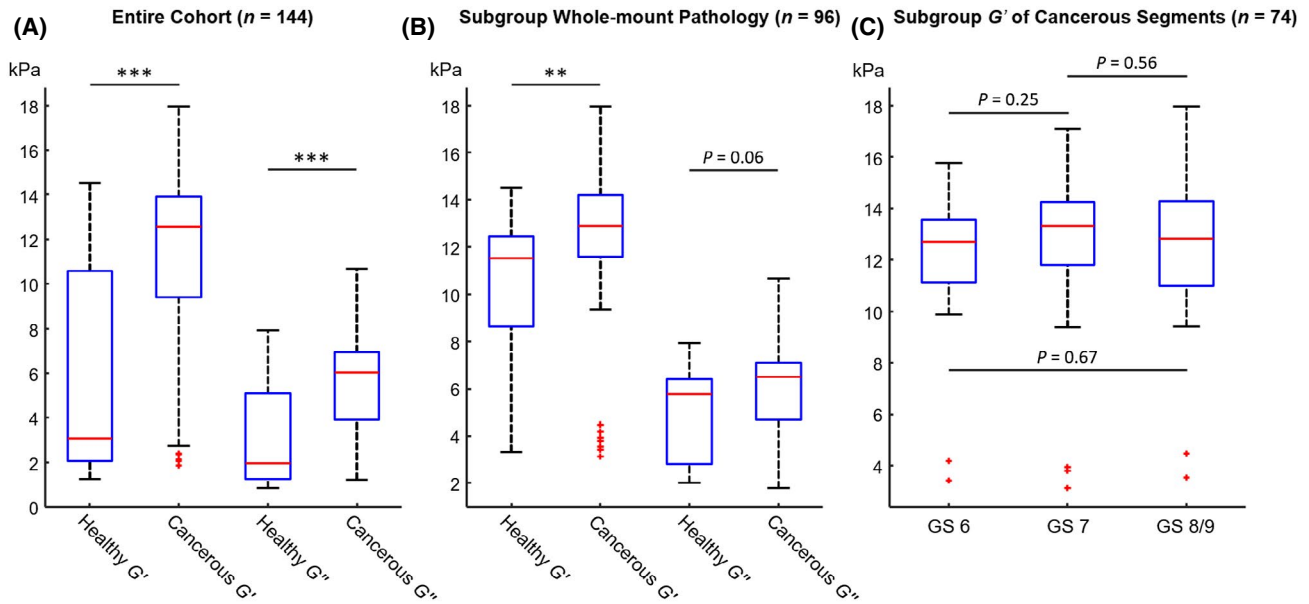


FIGURE 3 Boxplots show median, upper, and lower quartile, and whiskers of G' and G'' for healthy and cancerous segments of the entire cohort (A) and subgroup with whole-mount pathology (B). Additionally, values for different Gleason scores (GS) of the subgroup are displayed in (C). Statistically significant differences between groups are demarcated with asterisks: ** $P < .01$; *** $P < .001$

TABLE 4 Diagnostic performance of G' for the detection of prostate cancer

	Entire cohort (N = 144)	Subgroup whole-mount pathology (N = 96)		
	Any cancer (GS ≥ 6)	Any cancer (GS ≥ 6)	GS ≥ 7	GS $\geq 8/9$
Sensitivity	0.69 (0.61, 0.78)	0.61 (0.51, 0.71)	0.56 (0.46, 0.66)	0.36 (0.18, 0.56)
Specificity	0.79 (0.69, 0.87)	0.82 (0.68, 0.94)	0.78 (0.67, 0.89)	0.82 (0.75, 0.89)
NPV	0.62 (0.52, 0.72)	0.38 (0.27, 0.50)	0.53 (0.41, 0.63)	0.81 (0.74, 0.89)
PPV	0.84 (0.76, 0.91)	0.92 (0.85, 0.98)	0.81 (0.70, 0.90)	0.38 (0.20, 0.56)
AUC	0.81 (0.74, 0.87)	0.71 (0.62, 0.80)	0.65 (0.56, 0.74)	0.59 (0.46, 0.71)

Abbreviations: NPV, negative predictive value; PPV, positive predictive value.

4 | DISCUSSION

In this pilot study, we assessed the detection of PCa in fresh human prostatectomy specimens using MRE. We aimed to explore the potential of prostate MRE by overcoming current technical limitations using an ex vivo approach and improved SNR at 9.4 T. Shear stiffness was measured in 12 ex vivo prostates without formalin fixation or prior radiation therapy, and the diagnostic performance in detecting PCa based on tissue mechanical properties was assessed.

Overall, our results suggest a good diagnostic accuracy with AUC values of up to 0.81 for the detection of any PCa. The decrease in performance with increasing PCa grade might be attributed to similar stiffness values for low-grade, intermediate-grade, and high-grade PCa, where no significant differences were evident. A possible explanation for this finding could be the fact that PCa is not limited to a singular location like most other primary cancers, but spread out

through the entire organ with multiple foci and patterns of malignancy. This specific behavior of PCa is rarely reflected by mpMRI and only revealed in histopathological analysis in most cases. However, the finding of similar stiffness values for different PCa grades is preliminary and should be confirmed by larger studies in the future.

Although encouraging, we acknowledge that the performance of MRE alone in this study was inferior to already established in vivo methods such as diffusion MRI and transrectal ultrasound elastography, also bearing in mind the higher availability and lower cost of ultrasound. However, given that mpMRI has proven to improve biopsy outcomes and improve detection of high-grade PCa,¹⁸ adoption has increased significantly worldwide. As such, new adjunct MR sequences, such as MRE, deserve study because the incremental cost would become more favorable compared with non-MRI-based imaging. Other clinical utility advantages for MRI-based imaging are the potential for avoidance of biopsy

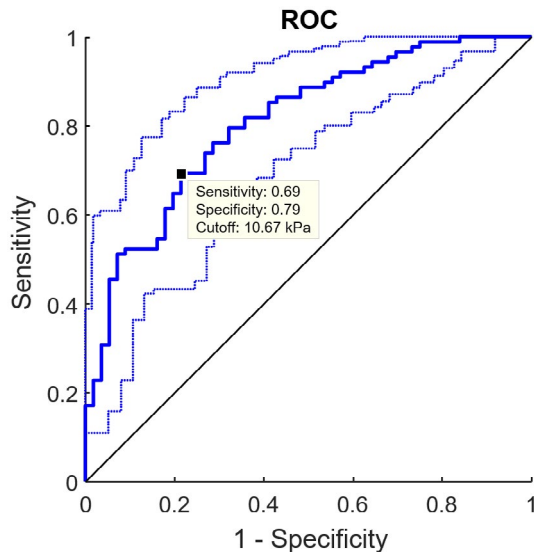


FIGURE 4 The receiver operating characteristic (ROC) curve shows the performance for the detection of any cancer ($GS \geq 6$) for the entire cohort. Dashed lines display the 95% confidence interval. The Youden index shows optimized values for sensitivity (69%) and specificity (79%) using a cutoff of 10.67 kPa. The area under the ROC is 0.81

and rectal ultrasound probes altogether if imaging protocols with sufficient negative predictive value could be developed.

4.1 | Comparison with in vivo mpMRI

A major limitation of mpMRI is its low specificity. In comparison to a recent in vivo mpMRI study by Ahmed et al, our preliminary results show a lower sensitivity (93% versus 69%) but an increased specificity (41% versus 79%).² The almost 2-fold increase in specificity is a stimulating result, which potentially might add value to in vivo scan protocols and improve differentiation of benign prostatic hyperplasia nodules from PCa. Of note, current standard mpMRI combines anatomic (T_2 -weighted), functional (DWI), and physiologic (DCE) assessment, whereas MRE relies on a single sequence. Another major limitation of mpMRI is interobserver variability. The current Prostate Imaging Reporting and Data System version 2.1 guidelines provide no clear definition of what constitutes mild, moderate, or marked restriction on DWI or hypointensity on T_2 -weighted imaging.¹⁹ Therefore, prostate MRE has the potential to improve diagnostic imaging and radiologic reporting as a quantitative imaging method.

4.2 | Comparison with other ex vivo MRE studies

As expected, the mean stiffness values of fresh prostatectomy specimens in our study were lower (healthy, 5.44 kPa;

cancerous, 10.84 kPa) compared with values reported in the literature: Dresner et al (formalin-fixed specimens): healthy = 11.89 kPa, cancerous = 21.52 kPa; Sahebjavaher et al (formalin-fixed specimens): healthy = 55-65 kPa, cancerous = 69 kPa; McGrath et al (prior radiation therapy and quasi-static MRE methodology): healthy = 48-99 kPa, cancerous = 85 kPa.^{6,7,9} Our results for G' were not distributed normally, with median values slightly higher than mean values, except for healthy segments of the entire cohort. An even more skewed distribution of stiffness values was found in a study by McGrath et al.⁶ These preliminary findings might be attributed to a small sample size and heterogeneous tissue based on different anatomic zones within the prostate, and the presence of benign prostatic hyperplasia nodules, fibrosis, and inflammation. Another finding of McGrath et al was that formalin fixation has a substantial effect on mechanical tissue properties, with a highly heterogeneous increase in stiffness up to 17-fold and a reduction of stiffness differences between healthy and cancerous tissue.⁶ Possibly, this might explain the lower diagnostic performance in PCA detection shown by Sahebjavaher et al with AUC values of 0.75 for the peripheral zone and 0.69 for the central gland.⁷ Our results did not show a correlation between stiffness and the age of men, which is in alignment with a study of Dresner et al.¹⁰

4.3 | Comparison with diffusion MRI

Rosenkrantz et al investigated the feasibility of in vivo diffusion kurtosis imaging for detecting PCa in the peripheral zone compared with standard DWI.²⁰ They showed an excellent performance for ADC (AUC, 0.93; sensitivity, 78.5%; specificity, 95.7%), which was even further improved using diffusion kurtosis imaging (AUC, 0.98; sensitivity, 93.3%; specificity, 95.7%). However, in a recent study including 285 patients with PCa, the same group found no clear benefit for diffusion kurtosis imaging (AUC, 0.90) in comparison to standard DWI (AUC, 0.92).²¹ In an ex vivo study, McGrath et al found no significant difference in ADCs between PCa and healthy tissue, although ADC values tended to be lower in PCa.⁶ Sahebjavaher et al directly compared the diagnostic performance of DWI and MRE in ex vivo specimens with fixation and found a lower performance for DWI (AUC, 0.68 versus 0.75).⁷ Moreover, a combined analysis of MRE parameters and DWI further improved performance (AUC, 0.82), suggesting that MRE and DWI provide complementary information. Finally, Uyanik et al reported initial experience with the use of stretched exponential model parameters of diffusion signal decay in 31 men for quantification of tissue heterogeneity and PCa classification.²²

4.4 | Comparison with ultrasound elastography

Promising results have also been reported by studies investigating transrectal ultrasound elastography. Correas et al investigated peripheral zone PCa detection in 184 men with elevated prostate-specific antigen or abnormal digital rectal examination results.²³ Of these men, 68 had positive biopsy findings, and ultrasound elastography showed excellent overall performance (AUC, 0.95; sensitivity, 96%; and specificity, 85%). Wei et al investigated a cohort of 212 men with clinically localized PCa using whole-mount prostatectomy specimens as reference standard and found an excellent diagnostic performance as well (AUC, 0.98; sensitivity, 97%; and specificity, 68%).²⁴

4.5 | Limitations

Our study has some limitations. First, a limitation arose from the short 2-hour period available for our experiments between surgery and pathology. In consultation with the pathologists, we aimed at preventing any potential damage of the fresh specimens without fixation, which could negatively impact histopathological analysis and further patient management. Due to this restriction in time, additional experiments for a comparison of diagnostic performance across other MRI methods such as multifrequency MRE for the fitting of rheological models, DWI, or diffusion kurtosis imaging could not be performed in this study. Second, an accurate 1-to-1 correlation and registration technique of tumor foci between MRI/MRE and whole-mount pathology slices remains challenging, primarily due to changes in volume and shape after surgical resection and during fixation.²⁵ Therefore, a segment-based approach was chosen for generating results, which are not subject to manual segmentation of multiple small tumor regions throughout the prostate. A limitation of this approach is that an anatomic segment of the prostate contains both transition and peripheral zones of the gland, which can contain unique nonmalignant pathology. Further development of a registering method between histologic tumor annotations and radiologic imaging is desirable but still in an experimental stage.²⁶⁻²⁸ Third, ex vivo imaging results differ from the results acquired under in vivo conditions; therefore, clinical applicability is limited. Contributing factors include (1) 9.4T magnet at room temperature versus 1.5T or 3T magnet at body temperature, (2) 500-Hz shear waves ex vivo versus 60-120 Hz in vivo, and (3) no surrounding soft tissue ex vivo versus substantial attenuation in a clinical setting. It is especially challenging that the small size of the prostate constitutes for higher mechanical frequencies, to see full wave periods in the order of the region of interest or smaller. High

frequencies in turn encounter more damping from the surrounding soft tissue. Furthermore, the implementation of a proportional-integral-derivative heating system to obtain specimen images at body temperature should be considered in future work, because stiffness tends to increase with decreasing tissue temperature. Still, the influence of room versus body temperature on tissue mechanical properties is expected to be a factor of only about 1.3, whereas tissue fixation causes variations of up to an order of magnitude.²⁹ Fourth, scan parameters such as TR, TE, and voxel resolution varied among specimens to account for different specimen sizes, and scan times were long in this experimental setting (Table 1). For instance, in certain cases (Table 1; prostates 3, 4, 5, 7, and 8), a larger number of image slices constituted higher TR values. To implement prostate MRE in a clinical setting, we plan to develop a standardized protocol with fast EPI sequences. Finally, the influence of prostatic inflammation and fibrosis remains unclear but should be addressed in future studies.

4.6 | Outlook

A recent study introduced a prostate-specific MRE setup with externally placed pressurized-air drivers, which provides an avenue for in vivo applications.³⁰ In the future, incorporation of prostate MRE into mpMRI protocols may improve PCa detection and staging and may offer a noninvasive alternative to transrectal prostate biopsy.

5 | CONCLUSIONS

This study provides preliminary results for the identification of PCa in fresh prostatectomy specimens without fixation or prior radiation therapy based on tissue mechanical properties. Especially the high value for specificity, in comparison to a current mpMRI study, is a stimulating result and encourages further investigation of this method as an adjunct MR sequence to already existing scan protocols. Our results suggest that prostate MRE has the potential to improve the diagnostic performance of mpMRI with special regard to its 2 major limitations: interobserver variability and low specificity.

ACKNOWLEDGMENTS

Support from the German Research Foundation is gratefully acknowledged. Preliminary results of this work were presented at the 26th Annual Meeting of the International Society for Magnetic Resonance in Medicine 2018.

ORCID

Rolf Reiter  <https://orcid.org/0000-0002-9741-6736>

REFERENCES

1. Muller BG, Shih JH, Sankineni S, et al. Prostate cancer: interobserver agreement and accuracy with the revised prostate imaging reporting and data system at multiparametric MR imaging. *Radiology*. 2015;277:741–750.
2. Ahmed HU, El-Shater Bosaily A, Brown LC, et al. Diagnostic accuracy of multi-parametric MRI and TRUS biopsy in prostate cancer (PROMIS): a paired validating confirmatory study. *Lancet*. 2017;389:815–822.
3. Ferlay J, Shin HR, Bray F, Forman D, Mathers C, Parkin DM. Estimates of worldwide burden of cancer in 2008: GLOBOCAN 2008. *Int J Cancer*. 2010;127:2893–2917.
4. Kvåle R, Møller B, Wahlqvist R, et al. Concordance between Gleason scores of needle biopsies and radical prostatectomy specimens: a population-based study. *BJU Int*. 2009;103:1647–1654.
5. Numao N, Kawakami S, Sakura M, et al. Characteristics and clinical significance of prostate cancers missed by initial transrectal 12-core biopsy. *BJU Int*. 2012;109:665–671.
6. McGrath DM, Lee J, Foltz WD, et al. MR elastography to measure the effects of cancer and pathology fixation on prostate biomechanics, and comparison with T1, T2 and ADC. *Phys Med Biol*. 2017;62:1126–1148.
7. Sahebjavaher RS, Nir G, Gagnon LO, et al. MR elastography and diffusion-weighted imaging of ex vivo prostate cancer: quantitative comparison to histopathology. *NMR Biomed*. 2015;28:89–100.
8. Good DW, Stewart GD, Hammer S, et al. Elasticity as a biomarker for prostate cancer: a systematic review. *BJU Int*. 2014;113:523–534.
9. Dresner MA, Cheville JC, Myers RP, Ehman RL. MR elastography of prostate cancer. In: Proceedings of the 11th Annual Meeting of ISMRM, Toronto, Canada, 2003. p 578.
10. Dresner MA, Rossman PJ, Kruse SA, Ehman RL. MR elastography of the prostate. In: Proceedings of the 10th Annual Meeting of ISMRM, Honolulu, Hawaii, 2002. p 460.
11. Arani A, Plewes D, Chopra R. Transurethral prostate magnetic resonance elastography: prospective imaging requirements. *Magn Reson Med*. 2011;65:340–349.
12. Arani A, Da Rosa M, Ramsay E, Plewes D, Haider MA, Chopra R. Incorporating endorectal MR elastography into multi-parametric MRI for prostate cancer imaging: initial feasibility in volunteers. *J Magn Reson Imaging*. 2013;38:1251–1260.
13. Sahebjavaher RS, Frew S, Bylinskii A, et al. Prostate MR elastography with transperineal electromagnetic actuation and a fast fractionally encoded steady-state gradient echo sequence. *NMR Biomed*. 2014;27:784–794.
14. Klatt D, Yasar TK, Royston TJ, Magin RL. Sample interval modulation for the simultaneous acquisition of displacement vector data in magnetic resonance elastography: theory and application. *Phys Med Biol*. 2013;58:8663–8675.
15. Klatt D, Johnson CL, Magin RL. Simultaneous, multidirectional acquisition of displacement fields in magnetic resonance elastography of the in vivo human brain. *J Magn Reson Imaging*. 2015;42:297–304.
16. Manduca A, Oliphant TE, Dresner MA, et al. Magnetic resonance elastography: non-invasive mapping of tissue elasticity. *Med Image Anal*. 2001;5:237–254.
17. Epstein JI, Egevad L, Amin MB, Delahunt B, Srigley JR, Humphrey PA. The 2014 International Society of Urological Pathology (ISUP) Consensus Conference on Gleason Grading of Prostatic Carcinoma. *Am J Surg Pathol*. 2016;40:244–252.
18. Kasivisvanathan V, Rannikko AS, Borghi M, et al. MRI-targeted or standard biopsy for prostate-cancer diagnosis. *N Engl J Med*. 2018;378:1767–1777.
19. Turkbey B, Rosenkrantz AB, Haider MA, et al. Prostate Imaging Reporting and Data System Version 2.1: 2019 Update of Prostate Imaging Reporting and Data System Version 2. *Eur Urol*. 2019;76:340–351.
20. Rosenkrantz AB, Lim RP, Haghghi M, Somberg MB, Babb JS, Taneja SS. Comparison of interreader reproducibility of the prostate imaging reporting and data system and likert scales for evaluation of multiparametric prostate MRI. *Am J Roentgenol*. 2013;201:612–618.
21. Tamada T, Prabhu V, Li J, Babb JS, Taneja SS, Rosenkrantz AB. Prostate cancer: diffusion-weighted MR imaging for detection and assessment of aggressiveness-comparison between conventional and kurtosis models. *Radiology*. 2017;284:100–108.
22. Uyanik M, Reiter R, Abern M, et al. Prostate cancer classification by using mono exponential, stretched exponential and kurtosis model parameters of diffusion signal decay. In: Proceedings of the 27th Annual Meeting of ISMRM, Montreal, Canada, 2019. p 3588.
23. Correas J-M, Tissier A-M, Khairoune A, et al. Prostate cancer: diagnostic performance of real-time shear-wave elastography. *Radiology*. 2015;275:280–289.
24. Wei C, Li C, Szweczyk-Bieda M, et al. Performance characteristics of transrectal shear wave elastography imaging in the evaluation of clinically localized prostate cancer: a prospective study. *J Urol*. 2018;200:549–558.
25. Groenendaal G, Moman MR, Korporaal JG, et al. Validation of functional imaging with pathology for tumor delineation in the prostate. *Radiother Oncol*. 2010;94:145–150.
26. Caldwell B, Uyanik M, Abern M, Macias V, Luciano C, Magin R. A methodology towards registering prostate histology and radiologic imaging to validate prostate cancer detection in 2D. In: Proceedings of the 26th Annual Meeting of ISMRM, Paris, France, 2018. p 3431.
27. Reynolds HM, Williams S, Zhang A, et al. Development of a registration framework to validate MRI with histology for prostate focal therapy. *Med Phys*. 2015;42:7078–7089.
28. McGrath DM, Lee J, Foltz WD, et al. Technical note: method to correlate whole-specimen histopathology of radical prostatectomy with diagnostic MR imaging. *Med Phys*. 2016;43:1065–1072.
29. Klatt D, Friedrich C, Korth Y, Vogt R, Braun J, Sack I. Viscoelastic properties of liver measured by oscillatory rheometry and multifrequency magnetic resonance elastography. *Biorheology*. 2010;47:133–141.
30. Dittmann F, Reiter R, Guo J, et al. Tomoelastography of the prostate using multifrequency MR elastography and externally placed pressurized-air drivers. *Magn Reson Med*. 2018;79:1325–1333.

How to cite this article: Reiter R, Majumdar S, Kearney S, et al. Prostate cancer assessment using MR elastography of fresh prostatectomy specimens at 9.4 T. *Magn Reson Med*. 2020;84:396–404.
<https://doi.org/10.1002/mrm.28127>